ac conductance of a magnetic multilayer structure with internal potential

Jie Yao,[1] Xuean Zhao,[1,2] Guojun Jin,[1,*] and Yuqiang Ma[1]
[1]*National Laboratory of Solid State Microstructures, Nanjing University, Nanjing 210093, China*
[2]*Zhejiang Institute of Modern Physics, Zhejiang University, Hangzhou 310027, China*
(Received 24 March 2003; published 7 August 2003)

The transport properties of a magnetic multilayer structure under a low-voltage and low-frequency perturbation are investigated. The theory is based on the ac linear response approximation developed by Büttiker *et al*. In the numerical calculations, the scattering matrix method is used. Also the calculations are self-consistent in order to take into account the internal potential caused by charge interactions inside the system. The numerical results reveal the transmission probabilities, dynamic admittance, and internal potential distributions under the changes of magnetic field and incident electron energy. The dc part and ac part of the conductance are dependent on the magnetic field strength, the size of the system, and the incident electron energy. In particular, the ac part of the conductance depends also on the wave-vector. This characteristic can be used to realize the wave-vector filtering device under ac perturbation. More interesting is that a transformation can be fulfilled between the inductive and capacitive behavior by tuning the magnetic field.

DOI: 10.1103/PhysRevB.68.054407 PACS number(s): 73.23.Ad, 73.61.−r, 73.40.Gk

I. INTRODUCTION

As the applications of nanostructure electronic devices increase rapidly in many fields, the electronic transport properties of small conductive structures are becoming more and more important. Pertinent researches, such as those on mesoscopic multilayered structures, experimentally and theoretically, have been carried out for a long time. The properties of conductance driven away from its steady state by time-dependent external perturbation has caused great research interest.[1,2] Transport of electrons in multiple-barrier magnetic structures under steady bias has been studied by many authors.[1,3–7] Theoretically, Matulis *et al.* pointed out that a magnetic multilayer structure has the property of wave-vector filtering for electrons passing through the structure.[1] Experimentally, Ye *et al.* investigated the periodic deposition of ferromagnetic microstructures on top of a high-mobility two-dimensional electron gas and found the magnetic commensurability oscillations.[8] The transport properties of a macroscopic counterpart for such a structure under time-dependent electric fields have also been explored classically.[9,10] It is intriguing and necessary to explore the effect of oscillating external perturbation on similar systems in a microscopic way. One of us (Zhao and Chen[11]) has investigated a nonmagnetic two-barrier system with the self-consistent approach which takes into account the internal potential caused by Coulomb interactions.

For magnetic fields perpendicular to the plane of carrier motion, one can alter the effective geometrical confinement on the carriers' transport by varying the magnetic fields and hence tune the functional dependence of the conductance on the magnetic field. Studying the conductance of quantum transport in a periodic magnetic field makes it possible to find important factors that affect the movement of carriers, including the parameters of the confining potential, charge accumulation, and wave-vector dependence, in the energy spectrum. Under the alternating external perturbation there is more physical information. Charge carriers will be affected by alternating electric field and confining magnetic field. To ensure current conservation and gauge invariance, carriers will absorb and emit phonons and the interaction between carriers must be considered.

Due to Büttiker's pioneering work, the low-frequency, gauge-invariant, and current conserved theory has been established in the scattering framework.[2,12,13] In this theory the partial density of states (PDOS) and the local partial density of states (LPDOS) (Refs. 14 and 15) play important roles. The dynamic properties of electron motion in mesoscopic systems are dominated by these partial densities of states. As one knows, the density of states (DOS) is used to describe the equilibrium properties of a physical system. In order to treat the nonequilibrium problems, the PDOS has been proposed to describe the dynamic properties such as injectivity and emissivity. The former describes carriers injected from a reservoir regardless to which reservoir the carriers exit, and the latter describes carriers emitted to a reservoir regardless from which reservoir the carriers enter. In fact, the PDOS is important in describing the ac conductance as will be discussed in the following section.

In this paper we are concerned about several issues for a magnetic multilayer structure, such as the transmission probability, the dynamic admittance, and the charge accumulation. Especially, the interesting wave vector as well as magnetic field dependences of ac conductance will be shown. The paper is organized as follows. The model and formulation are introduced in Sec. II; then in Sec. III the numerical work is done for several transport quantities, and the results are presented and discussed; in the last section a brief summary is given.

II. MODEL AND FORMULATION

A. General theory for linear ac conductance

We consider a mesoscopic structure with several terminals labeled by $\alpha, \beta, \gamma, \ldots$. If the chemical potential at terminal α is changed, such as applied an external perturbation, we can get the total current response at terminal β. For indepen-

dent electrons, the only potential energy an electron acquires is from external field. In the linear response theory, the conductance is determined by

$$g^{e}_{\alpha\beta}=\frac{1}{\hbar\omega}\int_0^\infty d\tau \exp[i(\omega+i0^+)\tau]\langle[\hat{I}_\alpha(\tau),\hat{I}_\beta(0)]\rangle, \quad (1)$$

where $\hat{I}_\alpha$ is the current operator which can be expressed by creation and annihilation operators $\hat{a}^\dagger,\hat{a}$ and $\hat{b}^\dagger$, $\hat{b}$, where $\hat{a}$ and $\hat{b}$ are related by a scattering matrix S—i.e., $\mathbf{b}=S\mathbf{a}$.

If the transport is in a steady state, the charge accumulation (or depletion) produces only electrostatic fields. In this case there is no current associated with excess charges. However, with a time-dependent perturbation the charge accumulation (or depletion) is always associated with displacement currents. In fact ignorance of electron-electron interactions makes Eq. (1) not satisfy the current conservation and gauge invariance. To ensure that the transport theory is current conserved and gauge invariant, Büttiker and co-workers[2,12,13,17] have developed an ac transport theory. The key notion in this theory is to consider a self-consistent internal potential induced by the piled-up charges. Therefore the interactions between electrons must be taken into account. Due to the internal interactions, an internal potential is formed. In the case of low voltage and in the Hartree approximation, the effective internal potential for an electron is

$$U(\mathbf{r},t)=\sum_\alpha u_\alpha(\mathbf{r})e^{i\omega t}\delta\mu_\alpha, \quad (2)$$

where $\delta\mu_\alpha$ is the variation of the electrochemical potential in reservoir α, while $u_\alpha(\mathbf{r})$ is the characteristic potential function.[12] The current response to this internal potential is through

$$g^{i}_{\alpha\beta}(\omega)=i\omega e^2\int dE\left(-\frac{\partial f}{\partial E}\right)\int d\mathbf{r}\frac{dn_\alpha(\mathbf{r})}{dE}u_\beta(\mathbf{r}), \quad (3)$$

where f is the Fermi distribution function in reservoirs and $dn_\alpha(\mathbf{r})/dE$ is called injectivity which describes the density of states of carriers that incident into probe α no matter which probe it goes out.

Combining Eq. (1) and Eq. (3), we can obtain the total ac conductance

$$g_{\alpha\beta}(\omega)=g_{\alpha\beta}(0)-i\omega e^2E_{\alpha\beta}. \quad (4)$$

In this formula, $g_{\alpha\beta}(0)$ represents the dc conductance of the system, while $E_{\alpha\beta}$ is characteristic of the ac response under an external oscillating perturbation, called *emittance*. In the Hartree approximation it can be expressed as

$$E_{\alpha\beta}=\int dE\left(-\frac{\partial f}{\partial E}\right)\int d\mathbf{r}\left[\frac{dn_{\alpha\beta}(\mathbf{r})}{dE}-\frac{dn_\alpha(\mathbf{r})}{dE}u_\beta(\mathbf{r})\right]. \quad (5)$$

At zero temperature, Eq. (5) can be reduced into

$$E_{\alpha\beta}=\int d\mathbf{r}\frac{dn_{\alpha\beta}(\mathbf{r})}{dE}-\int d\mathbf{r}\frac{dn_\alpha(\mathbf{r})}{dE}u_\beta(\mathbf{r}), \quad (6)$$

in which

$$\frac{dn_{\alpha\beta}(\mathbf{r})}{dE}=-\frac{1}{4\pi i}\left\{S^\dagger_{\alpha\beta}[E,U(\mathbf{r})]\frac{\delta S_{\alpha\beta}[E,U(\mathbf{r})]}{\delta U(\mathbf{r})}-\frac{\delta S^\dagger_{\alpha\beta}[E,U(\mathbf{r})]}{\delta U(\mathbf{r})}S_{\alpha\beta}[E,U(\mathbf{r})]\right\} \quad (7)$$

and $dn_\alpha(\mathbf{r})/dE=\Sigma_\beta dn_{\alpha\beta}(\mathbf{r})/dE$. For the complex conductance, Eq. (4), we can define its phase angle

$$\tan\theta=-\omega e^2E_{\alpha\beta}/g_{\alpha\beta}(0). \quad (8)$$

This definition is useful for investigating the capacitive or inductive properties of small quantum systems.

Because the internal potential is caused by the charge distribution, we can use the Poisson equation to calculate the characteristic potential distribution, i.e.,

$$-\nabla^2u_\alpha(\mathbf{r})+4\pi e^2\int d\mathbf{r}'\Pi(\mathbf{r},\mathbf{r}')u_\alpha(\mathbf{r}')=4\pi e^2\frac{dn_\alpha(\mathbf{r})}{dE}, \quad (9)$$

where $\Pi(\mathbf{r},\mathbf{r}')$ is the response function of charge density to electrostatic potential. As a simple case we use the Thomas-Fermi approximation $\Pi(\mathbf{r},\mathbf{r}')=dn(\mathbf{r})/dE\,\delta(\mathbf{r}-\mathbf{r}')$ to reduce the above equation to

$$-\nabla^2u_\alpha(\mathbf{r})+4\pi e^2\frac{dn(\mathbf{r})}{dE}u_\alpha(\mathbf{r})=4\pi e^2\frac{dn_\alpha(\mathbf{r})}{dE}, \quad (10)$$

in which $dn(\mathbf{r})/dE$ is the total DOS distribution. It is worth pointing out that we shall self-consistently compute the ac conductance for a mesoscopic structure. The self-consistency takes electron-electron interactions as a screening effect, so there will be a screening length λ_S in the computation. This is just the Thomas-Fermi screening length which is related to the DOS, i.e., $\lambda_S^{-2}=4\pi e^2dn(\mathbf{r})$/dE. So the screening length itself will join in the self-consistent calculation.

From these formulas we can study specific structures to obtain their dynamical conductances. One can see that the important quantities are the density of states and its components as well as the internal potential. These quantities can be obtained by solving the coupled Schrödinger equation and Poisson equation iteratively.

B. Electron in a magnetic multilayer

The system investigated here is shown in Fig. 1(a). It consists of a series of magnetic fields parallel (barrierlike) or antiparallel (well-like) with the z axis and arranged along the x axis in a range $[x_l,x_r]$, while in the y direction it is taken to be homogeneous. This structure is usually called a magnetic multilayer or magnetic superlattice.[1,16] There are two perfect leads connecting this magnetic multilayer to an external source and drain, labeled by contact 1 and contact 2. If an external alternating voltage is applied to the source, electrons will incident from one probe to the other experienced modulated magnetic fields. It is assumed that there are no magnetic fields in the leads. The vector potential distribution of this structure is shown in Fig. 1(b).

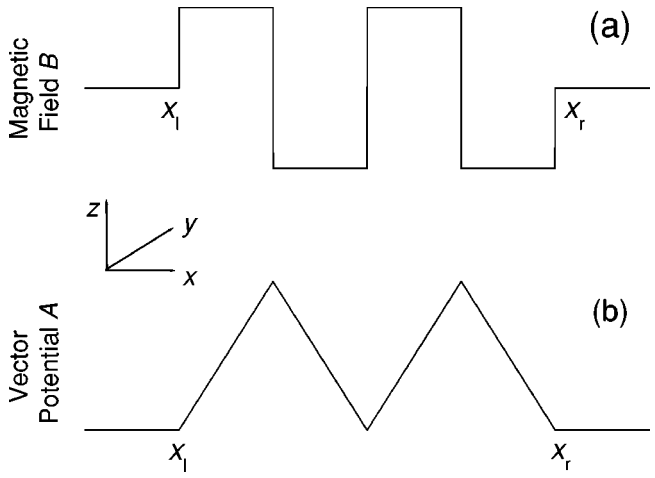

FIG. 1. Schematic drawing of a magnetic multilayer structure with the spatial distributions of magnetic field B (a) and vector potential A (b).

In the case for a two-dimensional gas that there exist an external magnetic field perpendicular to it and a small oscillating electric potential applied to it, the corresponding one-electron Hamiltonian reads

$$\mathcal{H}=\frac{1}{2m}[\mathbf{p}+e\mathbf{A}]^2+U(x)$$
$$=\frac{1}{2m}\{p_x^2+[p_y+eA(x)]^2\}+U(x), \tag{11}$$

where m is the effective mass of an electron, $\mathbf{A}=(0,\ A(x),0)$ is the vector potential in the Landau gauge, i.e., $A(x)=Bx$ or $-Bx$ piecewise continuously, $[p_y+eA(x)]^2/2m$ provides an equivalent magnetostatic potential, and $U(x)$ is the internal potential caused by the charge distribution. We can see that the y component of the momentum commutes with the Hamiltonian, i.e., $[p_y,\mathcal{H}]=0$. As a consequence we can write the wave function as $\Psi(x,y)=e^{iqy}\psi(x)$, where q represents the y component of a wave vector, later called the traverse wave vector. Thus we obtain the following one-dimensional Schrödinger equation involving the internal potential:

$$\left\{\frac{\hbar^2}{2m}\frac{d^2}{dx^2}-\frac{1}{2m}[eA(x)+\hbar q]^2-U(x)+E\right\}\psi(x)=0. \tag{12}$$

Because the applied field is low, the internal potential $U(x)$ is smoothly varied and can be expanded in a series. It can be written to the first three terms as

$$U(x+\Delta x)=U(x)+U'(x)\Delta x+\frac{1}{2}U''(x)\Delta x^2. \tag{13}$$

Using this expansion, the Hamiltonian can then be rewritten as

$$\mathcal{H}=-\frac{\hbar^2}{2m}\frac{d^2}{dx^2}+\frac{1}{2}m\omega^2(x-x_0)^2+C, \tag{14}$$

where

$$\omega=\frac{(e^2B^2+mU'')^{1/2}}{m}, \tag{15}$$

$$x_0=\frac{eB\hbar q-mU'}{e^2B^2+mU''}, \tag{16}$$

and

$$C=U(0)-E+\frac{1}{2m}\left[(\hbar q)^2+\frac{(eB\hbar q-mU')^2}{e^2B^2+mU''}\right]. \tag{17}$$

For convenience, we define a new variable

$$\xi=(m\omega/\hbar)^{1/2}(x-x_0) \tag{18}$$

and a new function

$$\psi(\xi)=P(\xi)\exp(-\xi^2/2). \tag{19}$$

According the above definition, we can rewrite Eq. (12) as

$$\frac{d^2P(\xi)}{d\xi^2}-2\xi\frac{dP(\xi)}{d\xi}+\lambda P(\xi)=0, \tag{20}$$

where $\lambda=2(E-C)/(h\omega)-1$. This is a standard Hermitian equation whose general solution is

$$P(\xi)=C_0P_0(\xi)+C_1P_1(\xi), \tag{21}$$

in which

$$P_0(\xi)=1+\frac{-\lambda}{2!}\xi^2+\frac{-\lambda(4-\lambda)}{4!}\xi^4+\cdots$$
$$+\frac{-\lambda(4-\lambda)\cdots(4n-4-\lambda)}{(2n)!}\xi^{2n}+\cdots \tag{22}$$

and

$$P_1(\xi)=\xi+\frac{2-\lambda}{3!}\xi^3+\frac{(2-\lambda)(6-\lambda)}{5!}\xi^5+\cdots$$
$$+\frac{(2-\lambda)(6-\lambda)\cdots(4n-2-\lambda)}{(2n+1)!}\xi^{2n+1}+\cdots. \tag{23}$$

Then we get the wave function immediately

$$\psi(x)=[C_0P_0(\xi)+C_1P_1(\xi)]\exp(-\xi^2/2). \tag{24}$$

The wave function of an electron beyond the magnetic region is just the superposition of plane waves propagating in the opposite directions, i.e.,

$$\psi(x)=A\exp(ikx)+B\exp(-ikx), \tag{25}$$

where $k=\sqrt{2mE}/\hbar$ and E is the energy of an electron. In the leads attached to the magnetic multilayer structure the incoming and outgoing wave functions are

$$\psi(x)=\begin{cases} e^{ik_l x}+re^{-ik_l x}, & x<x_l, \\ te^{ik_r x}, & x>x_r, \end{cases} \tag{26}$$

where r and t are the reflection and transmission amplitudes, respectively, $k_{l(r)}=\sqrt{2m(E-V_{l(r)})}/\hbar$, and $V_{l(r)}$ is the potential in the left (right) region of the structure, arising from the small deviation of chemical potential $\delta\mu_\alpha$.

C. Calculation scheme

For numerical calculations, we divide the system into very large number of small regions $s_1, s_2, s_3, \ldots, s_n$. The whole system is constructed by $s_1 \otimes s_2 \otimes s_3 \otimes \cdots \otimes s_n$. In each region, a uniform field is assumed. The electronic wave functions in different regions can be obtained by composing of the Hermitian function or the plane wave, such as

$$\psi_j(x)=A_j\phi_{j1}(x)+B_j\phi_{j2}(x), \tag{27}$$

where ϕ_{ji} can be either an Hermitian function or a plane wave. Between two adjacent regions, the continuum conditions of wave functions and their derivatives at the boundary result in a coefficient transfer matrix which connects the two couples of coefficients of the wave functions, i.e.,

$$\begin{pmatrix} A_j \\ B_j \end{pmatrix}=T_j\begin{pmatrix} A_{j+1} \\ B_{j+1} \end{pmatrix}. \tag{28}$$

At jth boundary, we have

$$M_j(x_j)\begin{pmatrix} A_j \\ B_j \end{pmatrix}=M_{j+1}(x_j)\begin{pmatrix} A_{j+1} \\ B_{j+1} \end{pmatrix}, \tag{29}$$

so $T_j=M_j^{-1}(x_j)M_{j+1}(x_j)$, where

$$M_j(x)=\begin{pmatrix} \phi_{j1}(x) & \phi_{j2}(x) \\ d\phi_{j1}(x)/dx & d\phi_{j2}(x)/dx \end{pmatrix}. \tag{30}$$

For the system $s_1 \otimes s_2 \otimes s_3 \otimes \cdots \otimes s_n$, we can obtain the global transfer matrix by multiplying all matrices T_j, i.e.,

$$T=\begin{pmatrix} T_{11} & T_{12} \\ T_{21} & T_{22} \end{pmatrix}=\prod_{j=1}^{n} T_j; \tag{31}$$

then the plane waves in the leads are connected by

$$\begin{pmatrix} e^{ik_l x_l} \\ re^{-ik_l x_l} \end{pmatrix}=T\begin{pmatrix} te^{ik_r x_r} \\ 0 \end{pmatrix}. \tag{32}$$

It is clear that one can get the transmission and the reflection coefficients by numerical calculations.

In addition one can also obtain the scattering matrix of the system. This can be realized by comparing the form of the transfer matrix and the scattering matrix

$$\begin{pmatrix} A_0 \\ B_0 \end{pmatrix}=T\begin{pmatrix} A_n \\ B_n \end{pmatrix} \tag{33}$$

and

$$\begin{pmatrix} B_0 \\ A_n \end{pmatrix}=S\begin{pmatrix} A_0 \\ B_n \end{pmatrix}. \tag{34}$$

The relationship between the elements of the scattering matrix and the transfer matrix is

$$\begin{pmatrix} S_{11} & S_{12} \\ S_{21} & S_{22} \end{pmatrix}=\begin{pmatrix} r_l & t_r \\ t_l & r_r \end{pmatrix}=\begin{pmatrix} T_{21}/T_{11} & T_{22}-T_{21}T_{12}/T_{11} \\ 1/T_{11} & -T_{12}/T_{11} \end{pmatrix}. \tag{35}$$

The ballistic dc conductance of a structure is directly related to the transmission probability

$$g_{21}(0)=\frac{2e^2}{h}T(E_F), \tag{36}$$

where E_F is the Fermi energy and $T(E_F)$ is the transmission probability of electrons with the Fermi energy.

The above discussion is based on the one-electron picture. As mentioned in the first part of this section, there are interactions between electrons in real circumstances, so we have to consider the interactions between electrons. The effective interaction of electrons is equivalent to an internal potential, which should be solved by a self-consistent numerical method. From the Schrödinger equation, we know that the wave function $\psi(x)$ is determined by the potential energy and, while from the Poisson equation, we see that the characteristic potential $u(x)$ is determined by the charge density distribution in the volume. According to the physical meaning of the partial density of state, the carriers' density can be obtained by

$$\frac{dn_\alpha(x)}{dE}=\frac{1}{hJ}|\psi_\alpha(x)|^2, \tag{37}$$

where $\psi_\alpha(x)$ is the scattering wave function incident from probe α and J is the incoming particle flux. By this partial density of states one can obtain the total DOS by summing up injectivities $dn_1(x)/dE$ and $dn_2(x)/dE$. Putting all these results into the Poisson equation (10), we obtain the characteristic potential $u_\alpha(\mathbf{x})$. Combining the internal potential with the equivalent magnetostatic potential, one gets a new potential in the Schrödinger equation. Solving the Schrödinger equation with the new effective potential, one obtains a new wave function. Since our structure is an open system, we have to use the transmission and reflection amplitudes to get the total wave function. With these self-consistent iterations to a necessary precision, we finally obtain the quantities needed.

In calculating the Poisson equation, we divide the structure into n small segments, each having a length Δx. Then we are able to make the Poisson equation discrete and transform Eq. (10) into the following solvable linear equation:

$$\begin{pmatrix} a_{11} & a_{12} & & & \\ a_{21} & a_{22} & a_{23} & & 0 \\ & & \ddots & & \\ & 0 & & & a_{n-1,n} \\ & & & a_{n,n-1} & a_{nn} \end{pmatrix} \begin{pmatrix} u_1 \\ u_2 \\ \vdots \\ \vdots \\ u_n \end{pmatrix} = \begin{pmatrix} d_1 \\ d_2 \\ \vdots \\ \vdots \\ d_n \end{pmatrix}, \tag{38}$$

where u_i is the discrete value of the potential in the ith segment and $d_i = 4\pi e^2 \Delta x^2 dn_\alpha(x_i)/dE$. The coefficient matrix is a tridiagonal matrix, in which $a_{i,i} = 4\pi\Delta x^2 e^2 dn(x_i)/dE + 2$, $a_{i,i-1} = a_{i,i+1} = -1$. The boundary condition is $u_1 = (1+R)/2$ on contact 1 and $u_n = (1-R)/2$ at contact 2, where $R = |r|^2$ is the reflection probability. The total internal potential $U(x)$ at point x in the Schrödinger equation is $U(x) = \Sigma u_\alpha(x) d\mu_\alpha$.

Using the expressions given above we can calculate the electronic transport properties of magnetic multilayer structures. We shall take the double magnetic barriers ($n=2$) and five magnetic barriers ($n=5$), as examples, to study their dc and ac properties.

III. RESULTS AND DISCUSSIONS

A. dc conductive properties

We first provide the numerical results for the transmission versus energy of a double magnetic structure with different system sizes in Fig. 2. The magnetic field strength is fixed at $B=1$ T. One can see that the transmission probabilities are exactly the same as those in the usual double-barrier structures when $q=0$. The corresponding magnetostatic potentials for these three different system sizes are shown in Fig. 3. Due to the magnetostatic potential from the magnetic field being about $U_B = (eBx)^2$, the larger the size of the system, the higher the potential as shown in Fig. 3, and the more bound states as shown in Fig. 2. The positions of the levels are the same in spite of the different level widths for each potential. This is due to the fact that the small potential is a part of the large potential which is clearly shown in Fig. 3. From Fig. 3 one can also see that the effective potentials are all finite harmonic potentials. It is confirmed that the energy spectra tend to the spectrum of a harmonic oscillator when the potential profile approaches the harmonic oscillator potential, as is shown in Fig. 2(d).

It is convenient to study the energy-dependent transmission and the internal potential distribution under different strengths of magnetic fields. Also from the fact that the magnetostatic potential U_B is related to the vector potential $A(x)$ which is the product of length L and magnetic field B, we can imagine that to increase the magnetic field may have the same effect as to increase the system length. Numerical results for $B=1$, 2, 3 T and fixed system length $L=200$ nm have confirmed this conjecture; i.e., the transmission probability and effective potential have almost the same profiles as in Fig. 2 and Fig. 3, respectively, although there are two differences: one is that the eigenenergies become denser as the magnetic field is larger; the other is that the higher potential has narrower well width, different from that of Fig. 3.

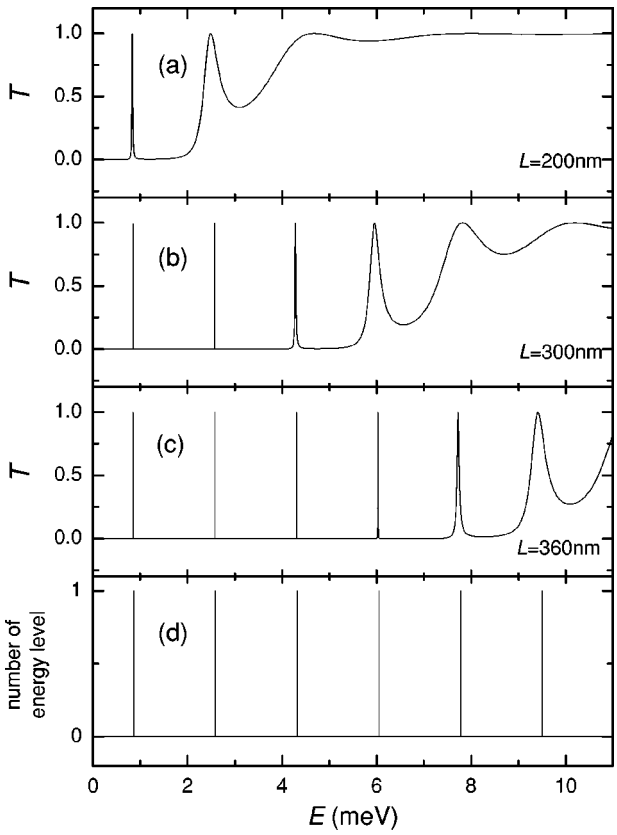

FIG. 2. Transmission probability T vs energy E for an incident electron in the case $n=2$ for different system lengths L, but a constant magnetic field ($B=1$ T). A comparison is made with the eigenenergies of a harmonic oscillator. (a) $L=200$ nm, (b) $L=300$ nm, (c) $L=360$ nm, and (d) the eigenenergy levels of a harmonic oscillator.

In the presence of a magnetic field, the equivalent magnetostatic potential $U_B(x) = [eA(x) + \hbar q]^2$ depends not only on the magnetic field, but also on the traverse wave vector. Therefore the transmission probability will be affected by the traverse wave vector q,[1,18] because the resonant levels will shift under the change of q. As indicated in Fig. 4, for some q there exist bound states and for other q there may not exist bound states, inside the magnetic field region. This charac-

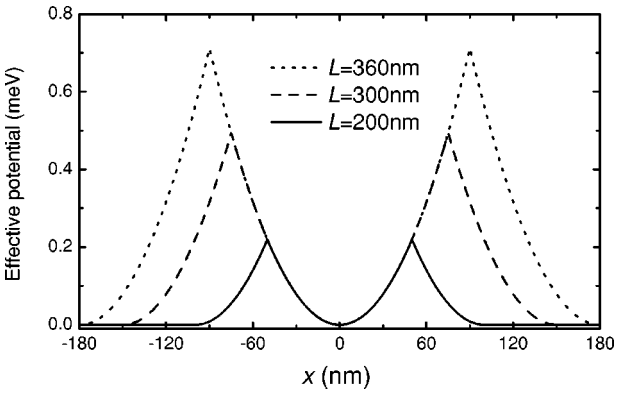

FIG. 3. Magnetostatic potential distributions for three systems with the different lengths corresponding to Fig. 2.

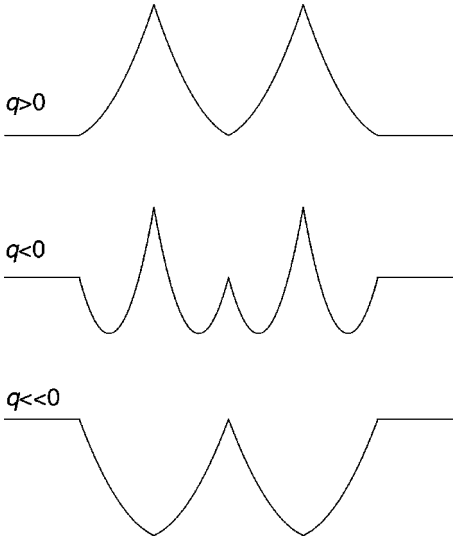

FIG. 4. Magnetostatic potential distributions with different traverse wave vectors.

teristic is different from the electric potential and can be used to adjust the effective potential by using the vector potential $A(x)$. The transmission spectra with different q are shown in Fig. 5. In order to make the effects of q more clearly, we plot T vs E_x instead of T vs E, where E_x is the longitudinal energy satisfying $E=E_x+\hbar^2q^2/2m$. The traverse-wave-vector-dependent shift of the resonant levels is clearly shown in Fig. 5.

We have also perform numerical calculations for five magnetic barriers. It can be found that each transmission peak in Fig. 2 will be split into 4. This is consistent with the rule of $(n-1)$ splitting for a n multibarrier structure.

B. Emittance

According to Eq. (4) the ac dynamic admittance is governed by the imaginary part of the conductance and an *emittance* is defined.[12] Figure 6 shows the emittance $E_{\alpha\beta}$ of a

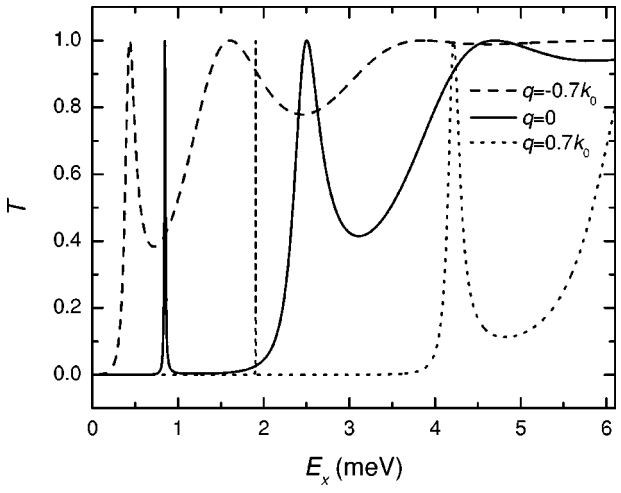

FIG. 5. Transmission probability T vs longitudinal energy E_x with the different traverse wave vectors in the case $n=2$, where $k_0=(2m\omega/\hbar)^{1/2}$.

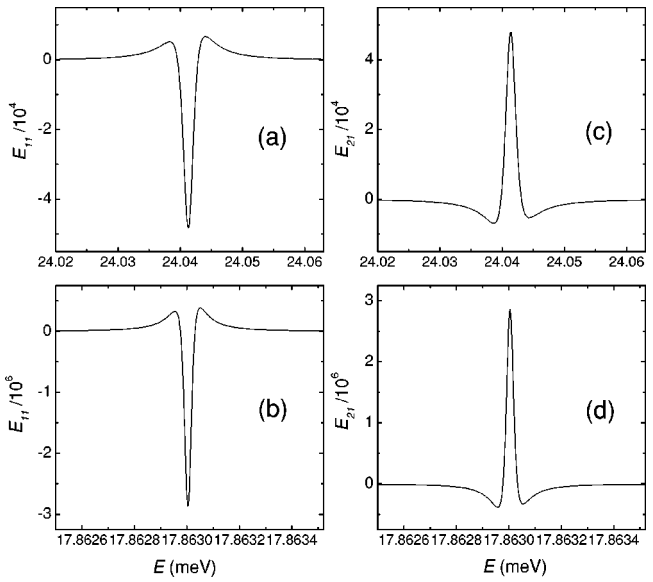

FIG. 6. (a),(b) Diagonal emittances E_{11} vs chemical potential E. (c),(d) Off-diagonal emittances E_{21} vs chemical potential E. In (a) and (c), the resonant energy is $E=24.0413$ meV, while in (b) and (d) the resonant energy is $E=17.8630$ meV.

system with magnetic field, $B=3$ T, and system length $L=200$ nm. These parameters lead to resonant peaks within the energy range from zero to top of the barriers. It will be helpful for us to understand the role of emittance by thinking of classical circuit elements, such as capacitor C and inductor L. Both appear in the imaginary part of a circuit conductance $g=g_0+i\omega X$, where X represents the dynamic admittance which is caused by the dynamic interaction between the charges. From the discussion in Sec. II, one sees that the emittance is a function of Coulomb interaction and magnetic field. In Figs. 6(a) and 6(b) are the diagonal emittances E_{11}, and in Figs. 6(c) and 6(d) are the off-diagonal emittances E_{21}. From Fig. 6 one sees that the large variations occur around the resonant energy.

The numerical results show that a diagonal emittance is negative when the Fermi energy of the reservoir is close to the resonant energy E_r. That is a inductive behavior. But it increases rapidly as the Fermi energy departs from the resonant energy and goes from negative to positive, and so shows the capacitive feature. After it reaches a maximum at each side of E_r it will slowly drops down and goes to zero asymptotically. This behavior for the emittance in a magnetic multilayer structure is similar to the theoretical results obtained by Prêtre *et al.* for electric multibarrier.[11,17] When E_F is close to E_r, the transmission probability is high. But this does not mean that electrons travel through the structure directly. It will dwell inside the system like an oscillator (we will discuss this phenomenon in Sec. III D). So the phase of the disturbance will be delayed through the system. This is a key characteristic of an inductance. If the incident energy is apart from the resonant energy E_r, the transmission probability becomes small. The electrons cannot travel through the system easily. Charges will be accumulated in the structure. The system behaves just like a capacitor. The emittance changes the sign from negative to positive.

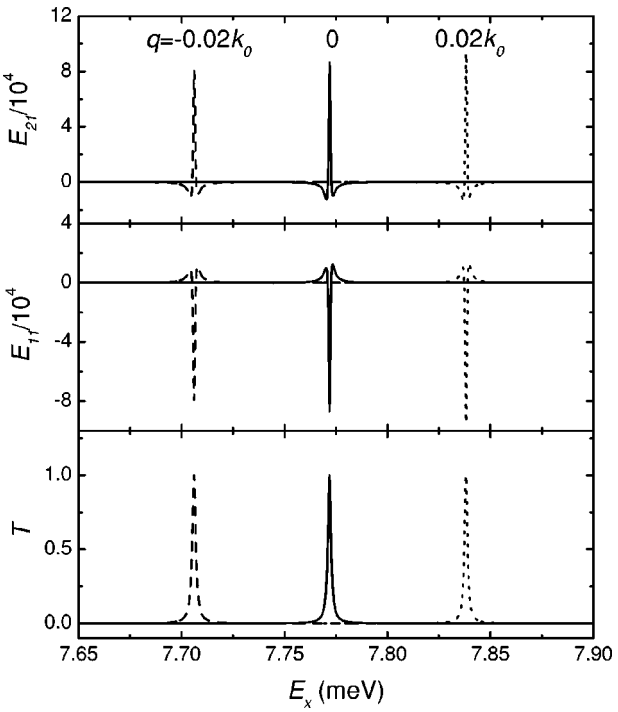

FIG. 7. Emittances E_{11} and E_{21}, compared with the transmission probability T, vs longitudinal energy E_x with three different traverse wave vectors q in the case $n=2$, where $k_0=(2m\omega/\hbar)^{1/2}$.

On the contrary, the off-diagonal emittances have an opposite shape with respect to the diagonal ones. Near a resonant energy, E_{21} has a positive peak; then it drops to negative values as the Fermi energy deviated from the vicinity of E_r. And it also has one minimum at each side of E_r corresponding to the two maxima of E_{11}. Two of us (Zhao *et al.*[19]) have calculated the off-diagonal emittance theoretically. And our numerical results here agree with the theoretical ones very well.

There is an interesting wave-vector filtering property for ac transport. As we calculate the emittance with different traverse wave vectors, it is found that, like in the dc case, the emittance is dependent on the wave vector q. From Eq. (5) one can see that the emittance is related to the PDOS and the internal potential. We know that the magnetostatic potential is $U_B(x)=[eA(x)+\hbar q]^2$. The shift and shape of peaks are dominated by this potential, and therefore determined by the wave vector q. From Fig. 3 one can see that $q>0$ corresponds to a double-barrier structure, while $q<0$ corresponds to a four-well structure. These potential structures indicate that the resonance occurs at lower positions for $q<0$ and higher positions for $q>0$. These results are clearly confirmed by our numerical calculations as shown in Fig. 7.

C. Spectrum versus magnetic field

For a fixed chemical potential, the conductance is a function of magnetic field B. We will explore the field-dependent properties for a double-magnetic-barrier structure.

The transmission probability T is shown as a function of magnetic field B in Fig. 8. As discussed before, one can see

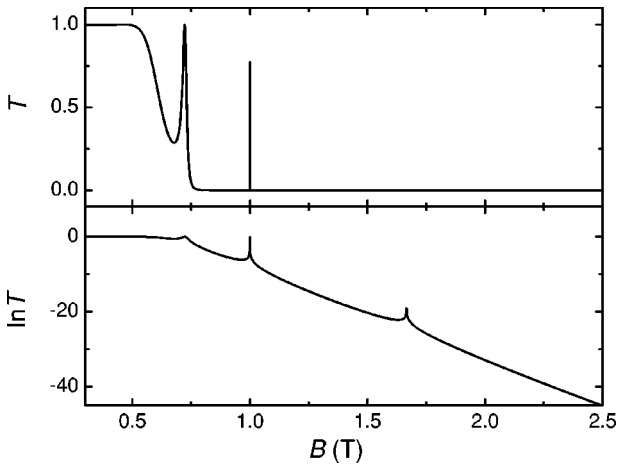

FIG. 8. Transmission probability T vs magnetic field B in the case $n=2$. $\ln T$ is plotted for clearness.

that as the magnetic field increases, the number of resonant energy levels also increases. So the curve in Fig. 8 can be explained as follows: When B is small, the barriers of the equivalent magnetostatic potential are low, and the electrons with a given energy, which is higher above the barriers, can pass through the structure easily; thus the transmission probabilities are near to 1. As the barrier height increases to a value which is larger than a given electron energy, the transmission probability T falls down quickly until the electron energy is near the highest intrinsic energy level of the structure, where T is a sharp peak in the T-B spectrum. The number of resonant energies and the level distance increase with the stronger magnetic field B. At last the lowest-energy level exceeds the energy of the incident electrons; there is no resonant level matching the incident energy, so there is no peak in the spectrum.

Figure 9 shows the emittances E_{11}, E_{21} and phase angle θ of the complex conductance $g_{21}(\omega)$ changing with magnetic field B and chemical potential E. The emittances and phase angle have the same zero point on the B axis and on the E axis which can be determined from the definition of the phase angle, Eq. (8). Here we take the frequency of the oscillating external perturbation $\omega=1$ GHz. The plot of the phase angle in Fig. 9 shows the transformation between the capacitive and inductive behavior of the structure. Around the resonant peak, the off-diagonal emittance E_{21} is positive as shown in Fig. 9(b) and the phase angle is negative in Fig. 9(c). These results indicate that the magnetic barrier structure possesses capacitive and inductive properties for different magnetic strengths. In the narrow width of a resonant peak, the structure behaves as an inductancelike property, and apart from the resonant peak, the structure has a capacitancelike property.

We show in Figs. 10 and 11 the transmission probability T, emittance E_{21}, and phase angle θ of the complex conductance $g_{21}(\omega)$ near the resonant energies for a five-period system. The system length is set to 600 nm. The quantities in Fig. 10 are all versus the variation of the chemical potential in the reservoir. Corresponding to the four resonant peaks in Fig. 10(a), the emittance in Fig. 10(b) also consists of four

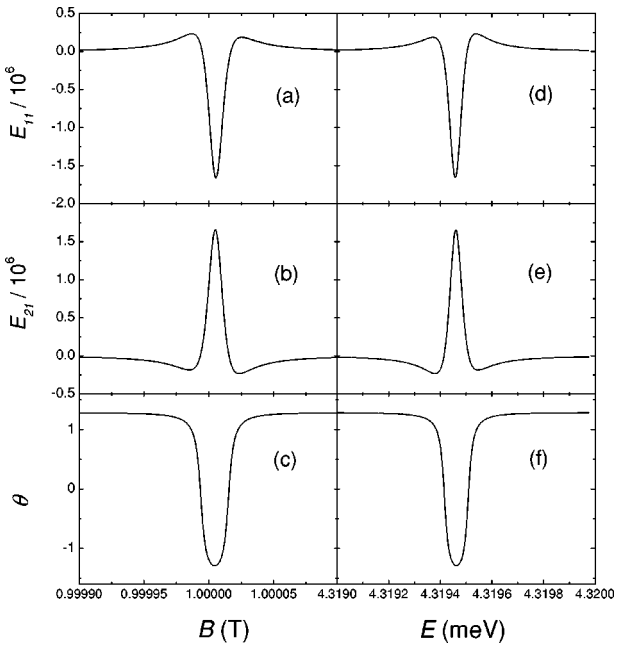

FIG. 9. Emittances E_{11}, E_{21}, and phase angle θ of the complex conductance $g_{21}(\omega)$ vs magnetic field B and vs chemical potential E in the case $n=2$.

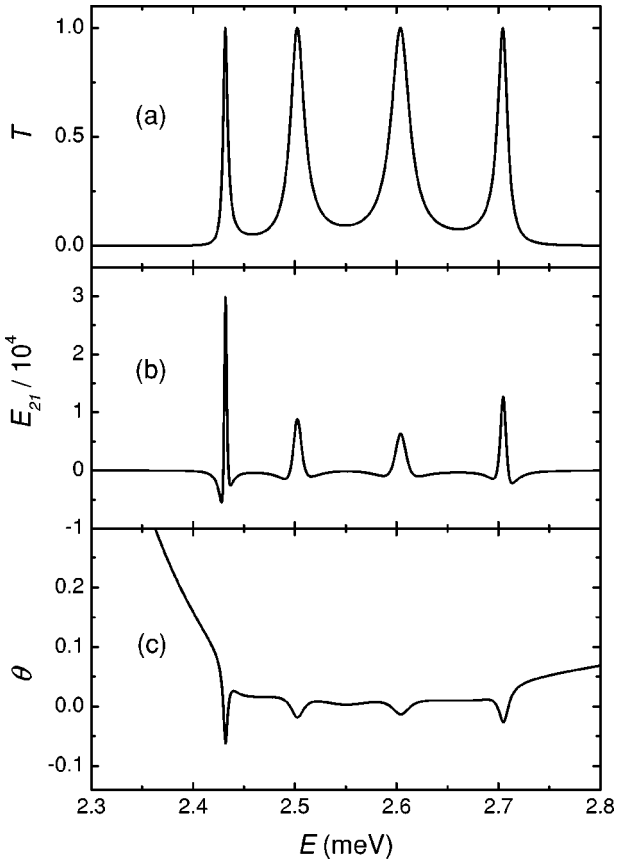

FIG. 10. Transmission probability T, off-diagonal emittance E_{21}, and phase angle θ of the complex conductance $g_{21}(\omega)$ vs chemical potential E near the resonant peaks in the case $n=5$.

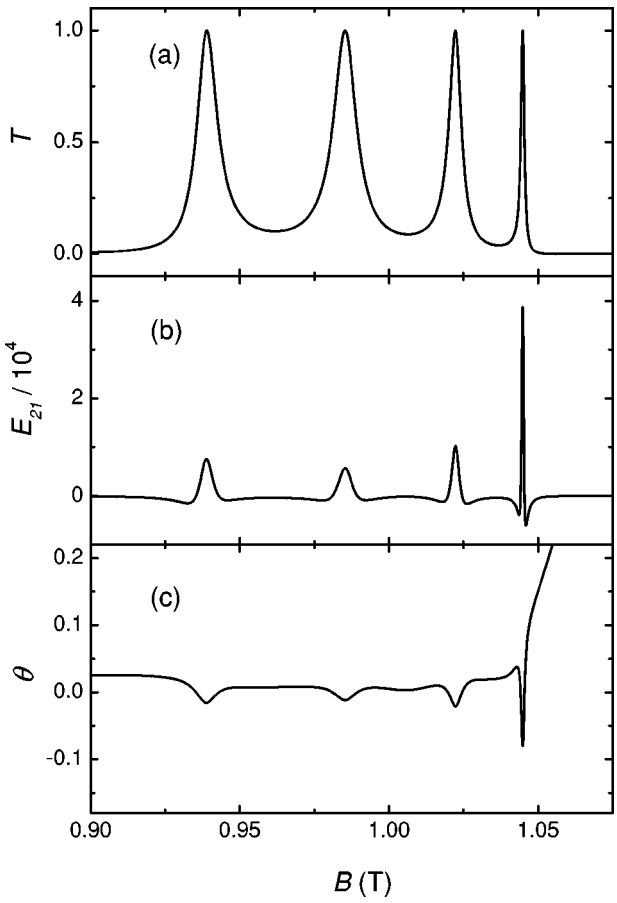

FIG. 11. Transmission probability T, off-diagonal emittance E_{21}, and phase angle θ of the complex conductance $g_{21}(\omega)$ vs magnetic field B near the resonant peaks in the case $n=5$.

peaks. Each peak is very similar to that of the two-period case. It seems that the emittance in the five-period case is just a combination of four parts of emittance in the two-period case. From the derivation we can see that the emittance is determined mainly by the phase angle of the complex transmission amplitude, so the results show that each of the four resonant peaks experiences a complete change in magnitude and phase angle. Each peak of the emittance in the energy band is different. The first and fourth peaks of the transmission probability are relatively narrow. Thus the corresponding parts in the emittance curve are larger, while the second and third peaks are smaller. The phase angle in Fig. 10(c) tells us that the characteristics of a device can be well regulated to change from inductive to capacitive, or vice versa, in a small energy range. This gives us a series of small inductive and capacitive ''windows'' which are arranged alternately. From the plot of the phase angle of the complex conductance, we can still recognize the difference between the five-period case and the two-period case. The phase angle is positive, but close to zero outside the four resonant regions; however, it decreases to lower than zero when the chemical potential locates in the middle of the resonant regions.

Figure 11 is also the results for a five-period case, but the relevant physical quantities are versus magnetic field B. From these figures we find that the results are very similar to

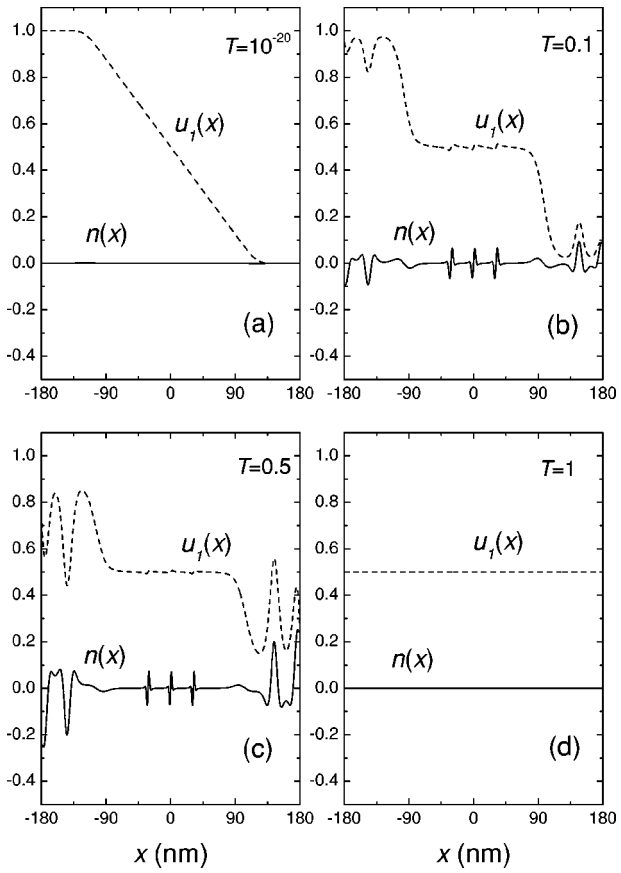

FIG. 12. Charge distributions $n(x)$ and characteristic potential distributions $u_1(x)$ for the cases with different transmission probabilities. (a) Very small transmission probability, (b) $T=0.1$, (c) $T=0.5$, and (d) $T=1$.

those discussed in Fig. 10. But these quantities change with magnetic field B in a direction opposite to those that change with energy E. The capacitive and inductive ''windows'' are also alternately arranged inside a certain range of field B. It is obvious that a multiperiod structure can give the sequential regulation of the inductive and capacitive property by chemical potential or magnetic field. However, a device may be more manipulable by changing the magnetic field than changing the chemical potential. This kind of a device may have many applications, such as to memory units.

D. Charge distribution and internal potential

As discussed in Sec. II, the interactions between electrons will induce a charge accumulation and give arise to an internal potential. We can calculate the internal potential for a magnetic multilayer structure. The internal potential gives an insight into the properties of a magnetic system under ac perturbation and reveals the meanings of physical quantities in magnetic fields. Figure 12 shows some charge distributions and characteristic potential profiles for a two-period magnetic structure.

It is clear that the charge distribution is related to the transmission probability. This is similar to the nonmagnetic double barrier case.[19,20] In Fig. 12(a) the transmission is very low and the charge density is very small inside the system. As T increases, charge piles up in the structure. But as E_F goes near the resonant tunneling energy E_r, the charge density decreases and there is almost no charge distributed inside the structure at resonance. This phenomenon can be easily understood. At low transmission, incident electrons cannot go inside the magnetic structure, so they can only pile up outside the potential near the two ends of the structure. But the accumulated charges are so small that we cannot see them obviously in Fig. 12(a). As T increases, electrons can go farther inside the structure, but they cannot all pass through the structure since the transmission probability is not 1. The charges jam in the magnetic field region and the charge density becomes large. Near the resonant energy, electrons pass through the structure without reflection so that few charges pile up inside the structure.

However, the resonance does not mean that electrons travel directly from one end to the other. This can be seen from the large density of electrons inside the potential well. Because our structure is formed by magnetic fields, electrons will convolute inside the magnetic field region before they go through the system. Thus the probability of electrons dwell inside the potential well is relatively large. This feature is consistent with the numerical results which show the increasing probabilities of electrons inside the magnetic potential well as the transmission probability increases.

Another special property in our magnetic structure is that the boundaries of the system are not so clear as for the nonmagnetic double barriers. For example, the potential profiles in these two cases are different, so that the charge accumulation in present case is not obvious as that in a nonmagnetic double-barrier structure. It makes the result more complicated, but we can still confirm the main characteristics of charge distribution.

In Fig. 12, the characteristic potential distribution $u_1(x)$ is also shown. At very low transmission, the potential profile is very simple. We would point out an important feature of this case: that the potential near two ends of the structure is rather flat. These regions can be regarded as the penetration depth as electrons can penetrate inside the system. The central part is just a straight line; it is also true at resonance, but the slope is different. When the transmission probabilities are neither very high nor very low, the potential profiles apart from the above extreme ones fluctuate drastically. These fluctuations are caused by the intricate charge distribution. The overall trend of potentials is decreasing from the left side to the right side. This is determined by the boundary conditions. We can see that as the reflection probability decreases, the potential profile tends to be flat, which proves the relation between the reflection probability and the boundary conditions of the internal potential.

IV. SUMMARY

We have studied the electronic transport properties of a magnetic multilayer structure under an alternating external perturbation based on the theory proposed by Büttiker *et al.* The internal potential arising from electron interactions has been taken into account. With an iterative calculation, the

coupled Schrödinger equation and Poisson equation were solved self-consistently. Some interesting results of the system were obtained. We have obtained the dc conductance which is consistent with previous works. The magnetic multilayer structure shows some similar properties with the common semiconductor multiwell structures. Yet it has its own special characteristics. What is more interesting is the ac part. By inspecting the charge distribution and internal potential distribution of the system, we can understand what happens inside the system that influences the overall electronic transport and gives explanations for the behavior of emittance. Corresponding to the filtering effect of the structure on transmission electrons with different wave vectors in the dc case, it has been found that the emittance is varied by the wave vectors of the incident electrons. The ac part acts just like the capacitance or inductance in classical circuits. And the results of our calculations indicate that it plays a very important role in the total conductance and can affect the features of our system greatly. For different Fermi energy or applied magnetic field, the emittance can behave inductively, or capacitively, which can be characterized by the phase angle of the total conductance. Because magnetic field is more manipulable in reality, these results are useful for designing new devices.

ACKNOWLEDGMENTS

This work was supported by The State Key Project of Fundamental Research Grant No. 001CB610602, NSF Grant No. 10274069, Zhejiang Provincial Natural Foundation Grant No. 500079, Natural Science Foundation of Jiangsu Province Grant No. BK200286, Educational Department of Zhejiang Province Grant No. G20010059, and SRF for ROCS, SEM. One of the authors (G.J.) is also grateful for the support of Grinnell College-Nanjing University Exchange Program.

*Author to whom correspondence should be addressed.

[1] M. Matulis, F.M. Peeters, and P. Vasilopoulos, Phys. Rev. Lett. **72**, 1518 (1994); I.S. Ibrahim and F.M. Peeters, Phys. Rev. B **52**, 17 321 (1995).

[2] M. Büttiker, J. Math. Phys. **37**, 4793 (1996); M. Büttiker and T. Christen, in *Quantum Transport in Semiconductor Submicron Structures*, Vol. 326 of *NATO Advanced Study Institute*, edited by B. Kramer (Kluwer Academic, Dordrecht, 1996), pp. 263–291.

[3] J.E. Müller, Phys. Rev. Lett. **68**, 385 (1992).

[4] H.A. Carmona, A.K. Geim, A. Nogaret, P.C. Main, T.J. Foster, M. Henini, S.P. Beaumont, and M.G. Blamire, Phys. Rev. Lett. **74**, 3009 (1995).

[5] Miguel Calvo, Phys. Rev. B **48**, 2365 (1993).

[6] V. Marigliano Ramaglia, A. Tagliacozzo, F. Ventriglia, and G.P. Zucchelli, Phys. Rev. B **43**, 2201 (1991).

[7] Y. Guo *et al.*, Phys. Rev. B **61**, 1728 (2000).

[8] P.D. Ye, D. Weiss, R.R. Gerhardts, M. Seeger, K. von Klitzing, K. Eberl, and H. Nickel, Phys. Rev. Lett. **74**, 3013 (1995).

[9] O.M. Yevtushenko and K. Richter, Phys. Rev. B **57**, 14 839 (1998).

[10] I.S. Ibrahim, V.A. Schweigert, and F.M. Peeters, Phys. Rev. B **56**, 7508 (1997).

[11] X. Zhao and Y.X. Chen, Phys. Rev. B **64**, 085326 (2001).

[12] M. Büttiker, J. Phys.: Condens. Matter **5**, 9361 (1993).

[13] M. Büttiker, A. Prêtre, and H. Thomas, Phys. Rev. Lett. **70**, 4114 (1993).

[14] V. Gasparian, T. Christen, and M. Büttiker, Phys. Rev. A **54**, 4022 (1996).

[15] Xuean Zhao, J. Phys.: Condens. Matter **12**, 4053 (2000).

[16] In fact, for a large fraction of the physics community, a magnetic multilayer is alternating layers of magnetic and nonmagnetic metals in which one finds such phenomena as the giant magnetoresistance. The present system which will be studied has spatially varying magnetic fields and also has been called magnetic multilayer in literature as we use here. It may be more appropriate to name it a magnetic-field-modulated structure.

[17] A. Prêtre, H. Thomas, and M. Büttiker, Phys. Rev. B **54**, 8130 (1996).

[18] F.M. Peeters and A. Matulis, Phys. Rev. B **48**, 15 166 (1993).

[19] X. Zhao, G. Jin, Q. Zhou, and Y. Li, Phys. Rev. B **66**, 045321 (2002).

[20] W.Z. Shangguan *et al.*, Phys. Rev. B **65**, 235315 (2002).